Paper submitted to the ANS Topical Meeting on Advances in Reactor Physics, March 8-11, 1992, Charleston, SC.

FEEDBACK COMPONENTS OF A U20PU10ZR-FUELED COMPARED TO A U10ZR-FUELED EBR-II

D. Meneghetti and D.A. Kucera

Reactor Analysis Division
Argonne National Laboratory
9700 S. Cass Avenue
Argonne, IL 60439
(708)972-6712

*Work supported by the U.S. Department of Energy, Nuclear Energy Programs under Contract W-31-109-ENG-38.

FEEDBACK COMPONENTS OF A U20Pu10Zr-FUELED COMPARED TO A U10Zr-FUELED EBR-II*

D. Meneghetti and D.A. Kucera
Argonne National Laboratory
Argonne, Illinois 60439

ABSTRACT

Calculated feedback components of the regional contributions of the power reactivity decrements (PRDs) and of the temperature coefficients of reactivity of a U20Pu10Zr-fueled and of a U10Zr-fueled Experimental Breeder Reactor II (EBR-II) are compared. The PRD components are also separated into power-to-flow dependent and solely power dependent parts. The effects of these values upon quantities useful for indicating the comparative potential inherent safety characteristics of these EBR-II loadings are presented.

INTRODUCTION

Calculational comparisons of detailed reactivity feedback components in regions of a U20Pu10Zr-fueled Experimental Breeder Reactor II (EBR-II) with the corresponding components of an analogous U10Zr-fueled EBR-II are made. These are of interest because of the planned conversion of the core to plutonium-containing fuel.

The linear and Doppler components comprising the power reactivity decrement (PRD) and the corresponding temperature coefficients of reactivity are calculated. The PRD at a power is here the negative of the reactivity required to bring the reactor from zero power hot-critical to that power. The PRD components are also separately delineated into power-to-flow dependent and into solely power dependent parts. These delineations together with the components of the temperature coefficients of reactivity are useful for indicating relative potential inherent safety characteristics.[1]

For each of the two fuel types three sets of components are calculated. These correspond at zero power, to: bond-sodium gap fully open; bond-sodium gap fully closed, the fuel not adhering to the clad, and no sodium in the fuel porosity; and bond-sodium gap fully closed, the fuel adhering to the clad such that the fuel axial expansion is that of the clad, and about one-third of the fuel porosity contains sodium.

---

*Work supported by the U.S. Department of Energy, Reactor Systems, Development and Technology, under contract W-31-109-ENG-38.

REACTOR LOADINGS

In these analyses the descriptions for the reactor are the same except for the fuel type, the cladding type, and a thicker cladding with a concomitant smaller radial dimension for the U20Pu10Zr fuel. Rows 1 to 6 of the reactor description constitute the core, rows 7 to 10 the radial steel reflector, and rows 11 to about 15 the radial blanket of essentially depleted uranium. The 91 subassembly locations in the cores contain: 62 drivers, 10 half-drivers, 8 operational control rods (7 high worth and 1 standard), 1 non-operational control rod experiment, and 2 safety rods. Also included in the six-rowed cores are: 1 fuel-type experiment, 3 structural-type experiments, and 5 dummy structural subassemblies.

The U20Pu10Zr driver fuel has 75% smear density (percentage of inner area of clad occupied by fresh fuel) and the Pu contains 81% Pu-239, 18% Pu-240, and 1% Pu-241. The fuel of 343 mm (13.5 in) length is contained in 5.84 mm (0.230 in) O.D. cladding having radial thickness 0.457 mm (0.018 in). The cladding of length 749 mm (29.5 in) and the 1.067 mm (0.042 in) diameter wire wrap are assumed to be made of HT-9, a ferritic steel. There are 61 fuel elements per driver subassembly. There are 31 fuel elements plus 30 steel elements per half-driver subassembly.

The U10Zr driver fuel has 75% smear density and a uranium enrichment of 67%. The fuel of 343 mm (13.5 in) length is contained in 5.84 mm (0.230 in) O.D. cladding having instead radial thickness of 0.381 mm (0.015 in). The 749 mm (29.5 in) long cladding and 1.067 mm (0.042 in) diameter wire wrap are assumed to be made of D2, an austenitic steel.

For both loadings the 61 elements of the control and safety rods are fueled by U10Zr with a uranium enrichment of 78%. The clad O.D. is 4.42 mm (0.174 in.), with radial thickness 0.305 mm (0.012 in). The fuel smear density is 75%. The remaining in core and out of core subassemblies are also considered to be identical in the two loadings.

METHODS

The linear and Doppler components of the PRDs are calculated using the EBRPOCO program[2] together with an addition (RODCO) to the program which estimates the PRD effects of axial positions of control rods. By repeating the calculation assuming all thermal conductivities to be infinite, the power-to-flow dependent components are obtained. (Setting the thermal conductivities in EBRPOCO to infinity causes the temperatures of all regions of a subassembly at a given axial level to have the same temperature above inlet as does the coolant at that axial level in the subassembly. Axial heat transfer in EBRPOCO is only by axial coolant flow.) The components of the power dependent part are obtained by subtraction of the calculated power-to-flow components from the corresponding components of the calculated PRD.

The components of the temperature coefficients of reactivity are calculated using the TEMCO addition[3] tc the EBRPOCO code. The grid-plate radial-expansion component of the temperature coefficient and some aspects of the net rod-bank suspension components of the temperature coefficient, which are additional

components of inlet temperature coefficients, are calculated separately from the EBRPOCO and TEMCO programs.

PRD COMPONENTS

For each core, steel radial-reflector, and uranium radial-blanket subassembly of a loading, the subassembly area-averaged axial distributions of the temperatures of sodium coolant, fuel-and blanket-element claddings, structural rods and steel reflectors, sodium in gaps, and fuel are calculated. Axially delineated PRD components for every subassembly and control rod location are calculated and then summed to obtain the regional components resulting from: coolant density (density reduction of Na due to temperature); coolant displacement (displacement of Na coolant by thermal expansion of cladding, structural rods, subassembly ducts and lower and upper axial reflector regions); steel density (density reduction of these steel components due to axial expansions with temperatures); bond Na (resultant of displacement of bond Na, if present in the open gaps, by differential thermal expansions of fuel and cladding and of density reduction of bond Na due to temperature or resultant of displacement of above-fuel bond Na, if present in close-gap situations, by thermal expansion of cladding and of density reduction of the above-fuel bond Na due to temperature); fuel and blanket axial expansions (free axial expansions if unrestricted by cladding or restricted axial expansion of fuel determined by axial expansion of cladding); Doppler (in fuel and blanket); and the rod-bank suspension (downward expansion of the control rods relative to core because of their being suspended from above).

The reactivity change resulting from a unit change in the core to rod-bank relative axial displacement, at the assumed rod-bank positions, is also calculated. It is subsequently used to obtain the net rod-bank suspension component of the inlet temperature coefficient by auxiliary calculations.

TEMPERATURE COEFFICIENT COMPONENTS

Because calculations of the components of the PRD using EBRPOCO require corresponding calculated axially-delineated temperatures of the intra-subassembly components, the temperatures are available for the calculations of corresponding temperature coefficients in the TEMCO addition to the program. In this manner temperature coefficients are calculated using a unified method following the EBRPOCO calculations of the PRD components. Temperature coefficients calculated by TEMCO correspond to average temperature coefficients between the coolant inlet temperature and the applicable positional temperatures at the power and coolant flow rate of the reactor.

NET ROD-BANK SUSPENSION COMPONENT

The effective rod-bank suspension component is the net reactivity resulting from the net effects of the axial movements of the control rods (because of their structural suspensions from above the reactor), the below core steel-containing regions and the surrounding sodium-containing pool tank (which is also suspended from above). This is a component of the coolant inlet temperature coefficient.

In EBR-II a steel vessel encloses the reactor subassemblies through which the primary coolant flows upward. The enclosed subassemblies rest upon a grid-plate region through which flows the inlet coolant pumped from the sodium pool

of the large surrounding overhead-suspended steel tank. The outer side of this tank is thermally insulated so that the tank wall at equilibrium is essentially at the temperature of the adjacent pool sodium. The vertical structural dimensions involved in these simplified and idealized analyses of the net rod-bank suspension components are schematically shown in Fig. 1. The arrows are directed to indicate directions of structural expansions resulting from temperature increases of the structures. For a change in coolant temperature due solely to change in inlet temperature and assuming the idealized equilibrium conditions that the temperature change occurs everywhere, including the pool sodium and the tank wall, the net rod-bank suspension coefficient in this situation is small because only the protrusion length of the fueled portion of the control rod is effective, i.e., $(l_u+l_v+l_p+l_a+l_g+l_s-l_t) = l_p$. (At the "11 in" rod-bank position the values of l_p are about 159 mm (6.25 in) for a high-worth control rod and 82.6 mm (3.25 in) for a standard control rod.)

The values of the reactivity changes resulting from unit change in the rod-bank to core net axial displacement at this banking (-0.1Δk/k per meter as calculated by RODCO) are used together with the effective averaged value of l_p and the thermal expansion coefficient of the steel to obtain the reactivity change per degree.

GRID-PLATE COMPONENT

The reactivity change resulting from radial expansion of the grid plate caused by a uniform change in its temperature is calculated by differences of the eigenvalues of the reference system and that of a uniform radial expansion of the system. The expansion of the grid plate causes voids in the system (everywhere above the grid plate) which are replaced by Na coolant of equivalent volumes. The grid-plate temperature coefficient component is the reactivity resulting from a one degree increase (only in its temperature) which causes the subassemblies to move radially outward because they set upon the grid-plate as a support. This component contributes to the coolant inlet temperature coefficient.

CONDUCTIVITIES AND EXPANSIONS

The thermal conductivities of the fuels over the temperature range of interest for these calculations are quadratic fits (as required by the EBRPOCO program) of estimates made from available data. For the U20Pu10Zr case these data are measured values[4] for U18.4Pu11.5Zr. For the U10Zr case these are interpolations of measured values[5] for U5Zr and U20Zr. Comparative values used herein for fresh fuels are listed in Table 1 at three temperatures. The fresh U20Pu10Zr conductivity is about 30 percent smaller than the fresh U10Zr conductivity.

The thermal conductivity of stainless steel assumed throughout these calculations is 12.0 $BTU \cdot hr^{-1} \cdot ft^{-1} \cdot F^{-1}$ (20.8 $W \cdot m^{-1} \cdot C^{-1}$) except in the axial regions of subassemblies having predominantly non-austenitic HT-9 steel. In the latter axial regions of those subassemblies the conductivity is increased to 15.0 $BTU \cdot hr^{-1} \cdot ft^{-1} \cdot F^{-1}$ (26.0 $W \cdot m^{-1} \cdot C^{-1}$). This is an averaged value over the temperature range of interest deduced from measured[6] data. Thus, the 25% increased value is used only in core and pintop axial-regions of the U20Pu10Zr fueled subassemblies in these analyses.

The fuel temperature coefficients of linear expansion assumed in these calculations are listed in Table 2 for the indicated temperature ranges. These are piecewise-constant approximate values (as required by the EBRPOCO program) deduced from expansion data[7] of U15Pu10Zr and U10Zr, respectively.

The temperature coefficient of linear expansion of stainless steels assumed in these calculations is $11.\times10^{-6}F^{-1}(20\times10^{-6}C^{-1})$ except in the axial regions of subassemblies having predominantly non-austenitic HT-9 steel. In the latter axial regions of those subassemblies the coefficient is reduced to 7.7×10^{-6} $F^{-1}(14.\times10^{-6}C^{-1})$. This value is an estimated average, for the range of interest, deduced from measured[6] data. Thus, the reduced value is used only in core and pintop axial-regions of the U20Pu10Zr fueled subassemblies in these analyses.

FEEDBACKS BY COMPONENTS AND REGION

The values are given in units of 10^{-5} $\Delta k/k$ and 10^{-7} $\Delta k/k$ per degree C for the reactivity components and the temperature coefficient components, respectively. The reactivity components are for a power of 62.5 MWt and total intrasubassembly (and intrarod) coolant flow of 8880 gpm ($0.560\ m^3\cdot s^{-1}$) corresponding to a discharge of about 9340 gpm ($0.590\ m^3\cdot s^{-1}$) from the primary pumps. The operational control rods are assumed at the "11 in" position. For conversions to β_{eff}-sensitive units values of 0.0053 and 0.0070, respectively, can be used for β_{eff}. In the tables the values in parentheses apply if at all powers the fuels in core are assumed to have the bond-sodium gaps fully closed (instead of fully open), however with the fuels not adhering to the clads and with no bond-sodium in the fuel porosities. The values in brackets apply if at all powers the fuels are assumed to be fully adhering to the clads, such that the axial expansions of the fuels are those of the clads, and about one-third of the resulting fuel porosities contain bond sodium.

PRD COMPONENTS

The regional contributions o the components of the PRDs are shown in Table 3 for the two fuel types designated as Pu and U. Except for core and above core regions the corresponding components are similar. The core values of fuel axial expansion components are larger in magnitude for the Pu-case than the corresponding U-case if the gaps are open or if the gaps are closed with fuels free to axially expand because of the smaller thermal conductivities for the Pu-case. If fuels are adhered to the clads this component is smaller in magnitude for the Pu-case because the temperature coefficient of the HT-9 steel clad is less than that of the austenitic steel clad of the U-case. The smaller negative values of the steel density component and the coolant displacement component also result largely from the same cause. These latter two components are analogously affected in the above core regions also because of the differing steel assumptions in the pintop axial-position of the overall above core region. For both the Pu- and U- cases the fuel axial expansion components are larger in magnitudes if the fuels are assumed to be expanded to the clads but not adhering thereto. This is especially noted for the Pu-case. These are because the porosities (due to burnup expansions) reduce the fuel conductivities and thereby increase the axial expansions.

The small negative Doppler values are relatively larger in magnitude for all three gap situations of the Pu-case relative to the corresponding U-case because of the larger U-238 content and larger temperatures of the fuel.

Sums over all components and regions result in ratios of the Pu-case values of the total linear (and Doppler) PRD relative to the values of the U-case of about 1.08, (1.23), and [0.95] for the three respective gap situations.

POWER-TO-FLOW COMPONENTS

The regional contributions of the power-to-flow components of the PRDs are shown in Table 4. The coolant density components, being solely power-to-flow dependent, are identical to those in Table 3. The rod-bank suspension components are assumed herein as essentially also power-to-flow dependent. The values of other components are smaller in magnitude relative to corresponding quantities of Table 3 because they represent reactivity losses resulting only from effects of the component temperature increases from inlet to the coolant temperatures at the various axial levels of the subassemblies. For the same reason the in core power-to-flow values of the Doppler components for the Pu-cases or the U-cases are not affected by closures of the bond-sodium gaps; and, the power-to-flow values of the fuel axial expansion components are also not affected by gap closures if the fuels, however, are not adhered to the clads.

It is noted that although various components of the Pu-case can noticeably differ from the U-case values, the sums over all components and regions result in ratios of the Pu-case to the U-case of only about 1.00, (1.00), and [0.95], respectively.

POWER COMPONENTS

The regional contributions of the power components of the PRDs are shown in Table 5. The power components of fuel axial expansion of core fuel (and associated bond-sodium component if present) and Doppler are significantly larger than values of corresponding power-to-flow quantities shown in Table 4. Values of coolant displacement and steel density quantities of power components for the radial steel reflector region are essentially as large as the corresponding power-to-flow quantities in Table 4. (This is because in EBR-II the steel in a radial reflector subassembly is in the form of a large hexagonal-shaped block, inserted into the hexagonal-shaped subassembly duct with the coolant flowing axially between the block and the duct. This results in sizeable radial edge-to-peak temperature differences which enhances the power components.)

Comparisons of the in core power components of the fuel axial expansion quantities for the Pu-case relative to corresponding U-case, in Table 5, indicate ratios of about 1.5 if the gaps are assumed fully open. These result from the larger fuel temperature in the Pu-case because of the relatively smaller conductivity. If the gaps are assumed closed but the fuels not adhering to the clads this ratio becomes 2.3. This is larger than the former ratio because the increased fuel temperature for the Pu-case increases the effective temperature coefficient of thermal expansion of that fuel more than for the U-case. The larger temperature encompasses a larger fraction of the expansion coefficient in the larger valued transitional region. If the fuels are assumed adhered to the clads then the power component, of the fuel axial expansion, of the Pu-case is

less than that of the U-case because of the lesser value of the temperature coefficient of the HT-9 steel clads relative to the austenitic steel clads.

Although sums of the power components over all regions moderate the effects of the large differences in the fuel components, significant differences can remain. Thus the ratios of the total linear (and Doppler) power components for the Pu-case relative to the U-case are about 1.3, (1.9), and [0.9], respectively.

TEMPERATURE COEFFICIENT COMPONENTS

The regional contributions of the components of the temperature coefficients of reactivity are shown in Table 6. Examination of the in core values for the Pu-cases relative to the U-cases show: less negative coolant density component due to the relatively smaller worth of sodium; less negative steel density component due to the presence of the smaller expansion of the HT-9 steel; less negative coolant displacement component due to the composite of the smaller expansion of the HT-9 steel and the lesser worth of the displaced sodium coolant; larger negative values of the fuel axial expansion, with fuels not adhering to the clads, due to the relatively larger fuel temperatures encompassing temperature ranges having the larger expansion rate with temperature; and more negative Doppler values due to the fuel composition having a larger U-238 content and which also then enhances the lower energy spectral shape by the increased inelastic-scattering. The effective net-rod-bank inlet-temperature coefficients are small; whereas, the grid-plate coefficients are large.

The values of the total inlet-temperature coefficients of the Pu-cases relative to the U-cases are only 1.03, (1.06), and [0.99] because of compensations of increasing and decreasing components.

INTEGRAL COEFFICIENTS AND FEEDBACK RELATIONS

Divisions of the sums of the components from Tables 3, 4, and 5, respectively, by the power give the integral coefficients of power (A+B), of power-to-flow (B), and solely of power (A). These together with the sums of the temperature coefficient components (C), from Table 6, are shown in Table 7. These integral coefficients enable the reactivity change $\Delta\rho$ due to a power increment ΔP, a power-to-flow increment $\Delta(P/Q^*)$, and a change ΔT_i in inlet-temperature to be approximated by $\Delta\rho \cong A\Delta P+B\Delta(P/Q^*) + C\Delta T_i$ where Q^* is the fraction of the reference flow. Listed are also corresponding quantities of interest in loss-of-flow-without-scram (LOFWS) and loss-of-heat-sink-without-scram (LOHSWS) situations assuming these loadings. For LOFWS the quantity A/B is significant because the ratio of the final coolant-temperature increment through the system at equilibrium conditions can for purposes of these intercomparisons be approximated by: $\Delta T_f/\Delta T_0 \cong 1+A/B$ where ΔT_f and ΔT_0 are the final and initial coolant-temperature increments across the system. For LOHSWS the quantity (A+B)/C is significant because the increase in coolant inlet-temperature required so that the negative reactivity will compensate for the otherwise positive reactivity resulting from the return of the PRD due to the power decrease to zero can be approximated by $\Delta T_i = (A+B)\ P/C$. (Non-inclusion of a subassembly bowing component in B should not significantly affect the LOFWS quantities. Non-inclusion of a subassembly-bowing component in B, however, most likely would cause the listed inlet coolant temperature increases, ΔT_i, to be too

large because in EBR-II the bowing component of the PRD is usually positive.) The quantity ϕ_0 (see footnote e. of Table 7) is significant because it is an indicator of the relative peak temperature overshoot in LOFWS situations in that if ϕ_0 is smaller the relative overshoot is larger and vice-versa.[1]

Thus, for situations having fuels not adhering to clads the U20Pu10Zr case has relatively larger $\Delta T_f/\Delta T_0$ (in LOFWS) and ΔT_i (in LOHSWS) values; but, for this case the relative values of ϕ_0 indicate less peak-temperature overshoot in LOFWS. For situations having fuels adhering to clads, however, the respective values of these quantities are essentially the same for the two cases.

CONCLUSIONS

Comparison of the feedbacks of the Pu-case relative to those of the U-fueled case result in the following main conclusions. (Percentage values in parentheses refer to approximate comparisons in β_{eff} units for the three assumed gap-situations.)

The PRD is about 20 percent larger for situations having fuels completely expanded to clads but not adhering to clads; but, the corresponding PRDs are within 10 percent for fully open gaps or for fuels adhering to the clads. (+40%, (+60%), [+25%])

The power-to-flow parts of the PRDs are similar for the corresponding gap situations. (+30%, (+30%), [+30%])

The power parts of the PRDs are 30 percent larger for the fully open gaps, 100 percent larger for the closed gaps having fuel free, and 10 percent smaller if the fuels are adhered to the clads. (+70%, (+150%), [+20%])

The inlet temperature coefficients of reactivity are similar. (+35%, (+40%), [+30%])

The LOFWS ratios $\Delta T_f/\Delta T_0$ are essentially similar except for the closed-gap fuel-free situations which indicate about a 20 percent increase.

The LOHSWS values of ΔT_i are similar except for the closed-gap fuel-free situations which indicate about a 15 percent increase.

The relative values of ϕ_0 indicate less peak-temperature overshoots during LOFWS.

REFERENCES

1. H.P. Planchon, J.I. Sackett, G.H. Golden and R.H. Sevy, "Implications of the EBR-II Inherent Safety Demonstration Test," Nucl. Eng. Des., 101, 75 (1987).

2. D. Meneghetti and D.A. Kucera, "EBRPOCO-A Program to Calculate Detailed Contributions of Power Reactivity Components of EBR-II," Proc. Int. Topl. Mtg. Advances in Mathematical Methods for the Solution of Nuclear

Engineering Problems, Munchen, FRG, April 27-29, 1981, Vol. 2, p. 225, Kernforschungszentrum Karlsruhe (1981).

3. D. Meneghetti and D.A. Kucera, "Calculation of the Temperature Coefficients of Reactivity for EBR-II Kinetic Analysis," Ann. Nucl. Energy, 14, 12, 663 (1987).

4. Reactor Development Program Progress Report, ANL-7230, 10 (1966).

5. Y.S. Touloukian, R.K. Kirby, R.E. Taylor, and P.D. Desai, "Thermophysical Properties of Matter, 1, Thermal Conductivity, Metallic Elements and Alloys", IFR/Plenum, New York (1970).

6. L. Leibowitz and R.A. Bloomquist, "Thermal Conductivity and Thermal Expansion of Stainless Steels D9 and HT9", Int. Journal Thermophysics, 9, No. 5, 873 (1988).

7. Y.S. Touboulian, R.K. Kirby, R.E. Taylor, and P.D. Desai, "Thermophysical Properties of Matter, 12, Thermal Expansion, Metallic Elements and Alloys," Plenum, New York (1975).

Table 1. U20Pu10Zr and U10Zr Thermal Conductivities
$BTU \cdot s^{-1} \cdot ft^{-1} \cdot F^{-1}$ $(W \cdot m^{-1} \cdot C^{-1})$

Fuel	700 F(371 C)	950 F(510 C)	1200 F(649 C)
U20Pu10Zr	0.0027(16.8)	0.0033(20.6)	0.0037(23.0)
U10Zr	0.0039(24.3)	0.0045(28.0)	0.0052(32.4)

Table 2. U20Pu10Zr and U10Zr Temperature Coefficients of Linear Expansion

Fuel	Temperature Range F(C)	Coefficient, Units 10^{-5} $F^{-1}(C^{-1})$
U20Pu10Zr	T<1112(600)	1.1(2.0)
	1112(600)≤T≤1224(662)	4.7(8.5)
	T>1224(662)	1.1(2.0)
U10Zr	T<1160(627)	1.0(1.8)
	1160(627)≤T≤1250(677)	6.0(10.8)
	T>1250(677)	1.2(2.2)

Table 3. Linear (and Doppler) PRD Components of a U20Pu10Zr-Fueled and a U10Zr-Fueled EBR-II, 10^{-5} Δk/k Units

Region	Fuel	Coolant Density	Coolant Displ.	Steel Density	Bond Sodium	Fuel Axial Exp.	Doppler	B_4C-Fuel	Sum
Core	Pu	-45.0	-9.7	-5.2	-15.1	-84.2	-6.7	0	-166.0
					(0)	(-146.3)	(-8.4)		(-214.6)
					[0]	[-23.6]	[-7.0]		[-90.5]
	U	-47.2	-13.6	-6.2	-14.2	-58.1	-4.8	0	-144.0
					(0)	(-72.3)	(-5.7)		(-145.0)
					[0]	[-30.4]	[-5.0]		[-102.3]
Above Core	Pu	-41.9	-6.7	-4.8	0	0	0	+1.2	-52.2
					(-16.0)				(-68.1)
					[-11.1]				[-63.3]
	U	-40.8	-9.0	-6.0	0	0	0	+1.2	-54.5
					(-16.2)				(-70.8)
					[-11.4]				[-65.9]
Below Core	Pu	-0.7	-0.5	-0.6	-0.2	-1.6	+1.5	0	-2.0
					(0)	(-2.0)	(+1.9)		(-1.9)
					[0]	[-1.7]	[+1.5]		[-1.9]
	U	-0.6	-0.5	-0.6	-0.1	-1.3	+1.2	0	-1.9
					(0)	(-1.6)	(+1.5)		(-1.8)
					[0]	[-1.4]	[+1.3]		[-1.7]
Rad. Refl.	Pu	-4.4	-6.8	-10.5	0	0	0	--	-21.7
	U	-4.4	-7.0	-10.5	0	0	0	--	-21.8
Rad. Blkt.	Pu	-0.3	-0.2	- 0.1	-0.1	-0.5	-1.7	--	-3.1
	U	-0.3	-0.2	-0.1	-0.1	-0.5	-1.6	--	-2.8
Sum	Pu	-92.3	-23.9	-21.2	-15.4	-86.4	-6.9	+1.2	-244.9
					(-16.1)	(-148.8)	(-8.3)		(-309.4)
					[-11.2]	[-25.9]	[-7.1]		[-180.4]
	U	-93.3	-30.2	-23.3	-14.5	-59.9	-5.1	+1.2	-225.1
					(-16.4)	(-74.5)	(-5.7)		(-242.1)
					[-11.5]	[-32.3]	[-5.3]		[-194.6]

Rod-bank Suspension Pu -57.3 U -56.0

Total Pu -302.2 (-366.7)[-237.7] U -281.2 (-298.1) [-250.6]

Table 4. Linear (and Doppler) Power-to-Flow Components of the PRDs of a U20Pu10Zr-Fueled and a U10Zr-Fueled EBR-II

Region	Fuel	Coolant Density	Coolant Displ.	Steel Density	Bond Sodium	Fuel Axial Exp.	Doppler	B_4C-Fuel	Sum
Core	Pu	-45.0	-7.3	-4.3	-6.4	-23.6	-2.2	0	-88.8
					(0)	(-23.6)	(-2.2)		(-82.4)
					[0]	[-16.1]	[-2.2]		[-74.9]
	U	-47.2	-9.9	-5.0	-6.1	-18.3	-1.7	0	-88.2
					(0)	(-18.3)	(-1.7)		(-82.1)
					[0]	[-20.4]	[-1.7]		[-84.1]
Above Core	Pu	-41.9	-6.7	-4.8	0	0	0	+1.2	-52.2
					(-16.0)				(-68.1)
					[-11.1]				[-63.3]
	U	-40.8	-9.0	-6.0	0	0	0	+1.2	-54.5
					(-16.2)				(-70.8)
					[-11.4]				[-65.9]
Below Core	Pu	-0.7	-0.1	-0.1	-0.1	-0.4	+0.3	0	-1.0
					(0)	(-0.4)	(+0.3)		(-0.9)
					[0]	[-0.4]	[+0.3]		[-0.9]
	U	-0.6	-0.1	-0.1	0.0	-0.3	+0.3	0	-0.8
					(0)	(-0.3)	(+0.3)		(-0.8)
					[0]	[-0.3]	[+0.3]		[-0.8]
Rad. Refl.	Pu	-4.4	-3.4	-5.4	0	0	0	--	-13.1
	U	-4.4	-3.4	-5.3	0	0	0	--	-13.0
Rad. Blkt.	Pu	-0.3	-0.2	-0.1	-0.1	-0.5	-1.6	--	-2.9
	U	-0.3	-0.2	-0.1	-0.1	-0.5	-1.4	--	-2.7
Sum	Pu	-92.3	-17.7	-14.7	-6.5	-24.5	-3.5	+1.2	-157.9
					(-16.1)	(-24.5)	(-3.5)		(-167.5)
					[-11.2]	[-17.0]	[-3.5]		[-155.1]
	U	-93.3	-22.6	-16.4	-6.2	-19.1	-2.9	+1.2	-159.3
					(-16.3)	(-19.1)	(-2.9)		(-169.4)
					[-11.5]	[-21.1]	[-2.9]		[-166.5]

Rod-bank Suspension Pu -56.6 U -55.3

Total Pu -214.5(-224.1)[-211.7] U -214.6(-224.7) [-221.8]

Table 5. Linear (and Doppler) Power Components of the PRDs of a U20Pu10Zr-Fueled and a U10Zr-Fueled EBR-II, 10^{-5} Δk/k Units

Region	Fuel	Coolant Density	Coolant Displ.	Steel Density	Bond Sodium	Fuel Axial Exp.	Doppler	B_4C-Fuel	Sum
Core	Pu	0.0	-2.4	-0.9	-8.7	-60.6	-4.5	0	-77.2
					(0)	(-122.7)	(-6.2)		(-132.2)
					[0]	[-7.5]	[-4.8]		[-15.6]
	U	0.0	-3.7	-1.2	-8.1	-39.8	-3.1	0	-55.8
					(0)	(-54.0)	(-4.0)		(-62.9)
					[0]	[-10.0]	[-3.3]		[-18.2]
Above Core	Pu	0.0	0.0	0.0	0	0	0	0.0	0.0
					(0.0)				(0.0)
					[0.0]				[0.0]
	U	0.0	0.0	0.0	0	0	0	0.0	0.0
					(0.0)				(0.0)
					[0.0]				[0.0]
Below Core	Pu	0.0	-0.4	-0.5	-0.1	-1.2	+1.2	0	-1.0
					(0)	(-1.6)	(+1.6)		(-1.0)
					[0]	[-1.3]	[+1.3]		[-1.0]
	U	0.0	-0.4	-0.5	-0.1	-1.0	+0.9	0	-1.1
					(0)	(-1.3)	(+1.2)		(-1.0)
					[0]	[-1.1]	[+1.0]		[-0.9]
Rad. Refl.	Pu	0.0	-3.4	-5.1	0	0	0	--	-8.6
	U	0.0	-3.6	-5.2	0	0	0	--	-8.8
Rad. Blkt.	Pu	0.0	0.0	0.0	0.0	0.0	-0.1	--	-0.2
	U	0.0	0.0	0.0	0.0	0.0	-0.2	--	-0.1
Sum	Pu	0.0	-6.2	-6.5	-8.9	-61.9	-3.4	0.0	-87.0
					(0.0)	(-124.3)	(-4.8)		(-141.9)
					[0.0]	[-8.9]	[-3.6]		[-25.3]
	U	0.0	-7.6	-6.9	-8.3	-40.8	-2.2	0.0	-65.8
					(-0.1)	(-55.4)	(-2.8)		(-72.7)
					[C.0]	[-11.2]	[-2.4]		[-28.1]

Rod-bank Suspension Pu -0.7 U -0.7

Total Pu -87.7(-142.6)[-26.0] U -66.5(-73.4)[-28.8]

Table 6. Components of Temperature Coefficients of Reactivity for a U20Pu10Zr-Fueled and a U10Zr-Fueled EBR-II, 10^{-7} Δk/k per °C Units

Region	Fuel	Coolant Density	Coolant Displ.	Steel Density	Bond Sodium	Fuel Axial Exp.	Doppler	B_4C-Fuel	Sum
Core	Pu	-77.2	-11.6	-7.00	-13.7	-45.4	-3.87	+1.07	-158
					(0)	(-58.5)	(-3.74)		(-157)
					[0]	[-30.8[a]]	[-3.85]		[-129]
	U	-82.3	-15.9	-8.03	-12.5	-34.6	-3.02	+1.25	-155
					(0)	(-35.1)	(-2.97)		(-143)
					[0]	[-38.0[a]]	[-3.01]		[-146]
Above Core	Pu	-38.3	-6.12	-4.63	0	0	0	+0.141	-49.0
					(-13.7)				(-62.6)
					[-9.52]				[-58.5]
	U	-37.1	-7.99	-5.72	0	0	0	+0.165	-50.6
					(-13.6)				(-64.3)
					[-9.56]				[-60.1]
Below Core	Pu	-34.6	-4.23	-5.96	-0.27	+1.32	+1.87	+0.490	-41.4
					(0)	(+1.32)	(+1.84)		(-41.2)
					[0]	[+1.32[b]]	[+1.85[b]]		[-41.0]
	U	-34.2	-4.18	-5.80	-0.266	+1.70	+1.76	+0.574	-40.3
					(0)	(+1.70)	(+1.74)		(-40.1)
					[0]	[+1.70[b]]	[+1.76[b]]		[-40.1]
Rad. Refl.	Pu	-17.1	-11.5	-18.0	0	0	0	-	-46.6
	U	-17.3	-11.7	-18.0	0	0	0	-	-47.0
Rad. Blkt.[a]	Pu	-0.727	-0.547	-0.342	-0.293	-1.09	-3.65	-	-6.65
	U	-0.763	-0.576	-0.355	-0.308	-1.11	-3.58	-	-6.69
Sum	Pu	-168	-34.0	-36.0	-14.2	-45.2	-5.65	+1.70	-301.
					(-14.0)	(-58.3)	(-5.55)		(-315)
					[-9.81]	[-30.6]	[-5.65]		[-283]
	U	-172	-40.3	-38.0	-13.1	-34.0	-4.84	+1.99	-301
					(-13.9)	(-34.4)	(-4.81)		(-301)
					[-9.87]	[-37.4]	[-4.83]		[-301]

Effective Net-rod-bank Inlet-temperature Coeff. Pu -3.24 U -3.24

Grid-plate Inlet-temperature Coeff. Pu -174. U -160.

Total Pu -478(-492)[-460] U -464(-464)[-464]

[a]Open-gaps assumed in blanket elements.
[b]Gaps-closed fuels-free and Na in one-third of porosities assumed in control rod fuels.
[c]Relative to clad temperature. (Relative to fuel temperatures this would effectively be -12.9)
[d]Relative to clad temperature. (Relative to fuel temperatures this would effectively be -17.2)

Table 7. Power, Power-to-Flow, and Inlet-Temperature Integral Coefficients and Pertinent LOFWS and LOSHWS Quantities

Case	Coefficient or Quantity	Open-Gap	Closed-Gap Fuel-Free	Closed-Gap Fuel-Restr. Na in ½ Pores
U20Pu10Zr-Fueled ($\beta_{eff} \cong 0.0053$)	(A+B)[a]	-4.83 (-0.91)	-5.87 (-1.11)	-3.81 (-0.72)
	B[a]	-3.44 (-0.65)	-3.58 (-0.68)	-3.39 (-0.64)
	A[a]	-1.39 (-0.26)	-2.29 (-0.43)	-0.42 (-0.08)
	C[b]	-4.78 (-0.90)	-4.92 (-0.93)	-4.60 (-0.87)
	$(\Delta T_f/\Delta T_0)$[c]	1.40	1.64	1.12
	ΔT_i[d]	63	75	52
	ϕ_0[e]	0.45	0.64	0.28
U10Zr-Fueled ($\beta_{eff} = 0.0070$)	(A+B)	-4.50 (-0.64)	-4.77 (-0.68)	-4.01 (-0.57)
	B	-3.44 (-0.49)	-3.60 (-0.51)	-3.55 (-0.51)
	A	-1.06 (-0.15)	-1.17 (-0.17)	-0.46 (-0.06)
	C	-4.64 (-0.66)	-4.64 (-0.66)	-4.64 (-0.66)
	$(\Delta T_f/\Delta T_0)$	1.31	1.33	1.13
	ΔT_i	61	64	54
	ϕ_0	0.29	0.32	0.23

[a]Units of 10^{-5} Δk/k per MWt (Units of cents per MWt).

[b]Units of 10^{-5} Δk/k per °C (Units of cents per °C.)

[c]$\Delta T_f/\Delta T_0 = 1 + (A/B)$.

[d]$\Delta T_i = (A+B)P/C$ in °C, P = 62.5 MWt.

[e]$\phi_0 = \frac{-\lambda\tau}{\beta_{eff}} \frac{(A+B)^2 P}{B}$ in $, λ=0.08s^{-1}, and τ=7s.

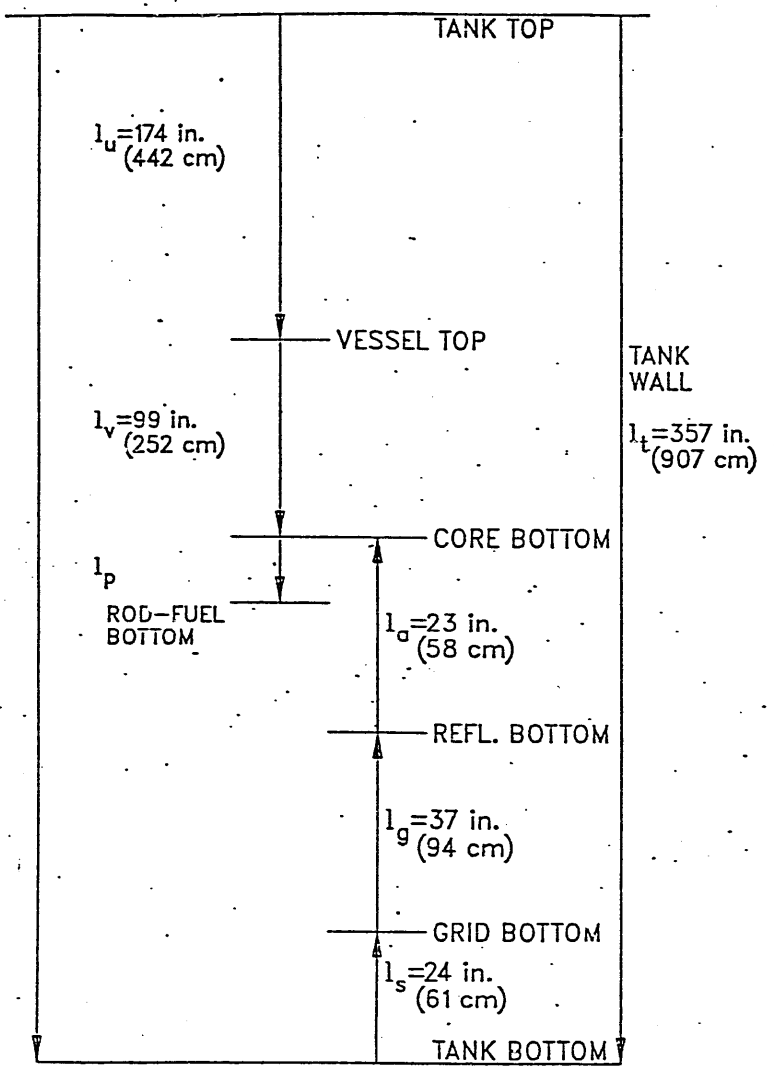

Fig. 1. Schematic diagram of vertical dimensions effective in net rod-bank suspension component (not to scale).

END

DATE FILMED

3/10/92